Influence of Copper-Impregnated Basic Oxygen Furnace Slag on the Fresh- and Hardened-State Properties of Antimicrobial Mortars

Ismael Justo-Reinoso [a,b], *Mark T. Hernandez* [b], and *Wil V. Srubar III* [b, c, 1]

[a] BRE Centre for Innovative Construction Materials, University of Bath, 6 East Claverton Down, Bath, BA2 7AY, UK. [b] Department of Civil, Environmental, and Architectural Engineering, University of Colorado Boulder, ECOT 441 UCB 428, Boulder, CO 80309-0428, USA. [c] Materials Science and Engineering Program, University of Colorado Boulder, 4001 Discovery Drive, Boulder, CO 80303, USA.

Abstract

Microbially induced concrete corrosion (MICC) is recognized as one of the main degradation mechanisms of sewer infrastructure worldwide. To help control this problem, a beneficial reuse path for basic oxygen furnace slag (BOFS) has emerged in which the incorporation of copper-laden BOFS particles into cementitous materials inhibits the growth of microorganisms responsible for MICC. The effect of substituting fine aggregate with copper-laden BOFS particles (0.30-0.85 mm) on the hydration and microstructural evolution of portland cement mortars is reported, and the fate of copper in the cured cementitious matrix is elucidated. As revealed by isothermal calorimetry, the total evolved heat at the end of the testing period (118 h) was similar when up to 40% of the fine aggregate mass was replaced with copper-laden BOFS particles of similar size, while delays in setting times were observed. Analysis of microstructural evolution using quantitative X-ray diffraction (QXRD) showed higher C-S-H contents when fine aggregate was replaced with copper-laden BOFS, indicating copper-laden BOFS exhibited some degree of pozzolanic reactivity. Electron microprobe analysis (EMPA) revealed that, while trace amounts of copper could be detected throughout the cement matrix, copper was predominantly localized in a 100 µm spherical region surrounding BOFS particles. Moreover, strong binding capacity of Fe-rich BOFS particles for copper was observed. Finally, compressive strengths of mixtures analyzed herein were not affected by the presence of copper-laden BOFS.

Keywords: Antimicrobial mortar; BOFS; copper; isothermal calorimetry; electron microprobe analysis; MICC.

[1]Corresponding author at: 1111 Engineering Drive, ECOT 441 UCB 428, Boulder, CO 80309, USA. T+1 303 492 2621
e-mail address: wsrubar@colorado.edu

1. Introduction

With an annual production of 1,816 million tonnes [1], the steel industry generates a large amount of solid byproducts, most notably, basic oxygen furnace slag (BOFS). Steel slag is a gravel-like residual discarded after a desired metal has been separated from its ore. Depending on the steelmaking process, steel slags will have different physicochemical properties. Oxygen furnaces produce low-carbon steel and discard between 363 and 454 million tonnes of BOFS annually [2, 3].

The United States, Germany, and Japan have found multiple ways to reuse certain slags, some of which approach repurposing rates close to 100% [4]. In contrast, many other countries do not repurpose BOFS, and it is considered a dead-end waste. For example, China is responsible for approximately half of the world's steel production and generates large amounts of BOFS that do not currently have reuse avenues [4]. Therefore, finding new beneficial reuse pathways for BOFS is economically and environmentally desirable. BOFS, either in powder or granular form, have been included in cement formulations for various purposes [2, 4-7]. One emerging application of BOFS in its granular form concerns metal-impregnated BOFS particles that have been used as a new class of antimicrobial admixture for inhibiting microbially induced concrete corrosion (MICC) [8-10].

Biogenic corrosion is a ubiquitous, now classic, phenomenon that threatens wastewater infrastructure worldwide. Comprehensive reviews on the topic are available [11-14]. MICC includes a variety of processes by which sulfur-oxidizing microorganisms (SOMs) contribute to accelerated corrosion of concrete sewers and wastewater appurtenances, which has serious economic and environmental consequences [11]. Caicedo-Ramirez *et al*. [15] showed that the growth of the most common SOMs associated with corroding sewers, *Acidithiobacillus spp.,* could be inhibited by low-level exposures to heavy metals—including copper—sorbed onto activated carbon particles. The antimicrobial effects of copper is based on its reactions with the negatively charged cell walls of bacteria and associated formation of complex compounds within the bacterial membrane [11]. Within recent years, antimicrobial admixtures containing different heavy metals have been increasingly used in conventional concretes in efforts to stem MICC proliferation [11, 16]. Two specific carriers have been previously reported for this metal-delivery purpose: zeolites [17, 18] and activated carbon [9, 10, 15, 19, 20]. In this context, the use of

copper-laden BOFS particles in cementitious materials represents a promising new approach to inhibit the microbes responsible for biogenic corrosion [8-10]. Even though the incorporation of copper-laden BOFS particles in cementitious materials has demonstrated a potent antimicrobial effect [8], how these BOFS inclusions specifically influence cement hydration and the mechanical properties of concrete remains unknown.

Cement hydration involves complex interactions that may be influenced either by the mineral composition of BOFS particles, by the presence of metals impregnated in them (*i.e.*, Cu), or both. As previously discussed, the characteristics and composition of BOFS vary depending on the ore and metal scrap used in the process, if any [2, 21]. The most abundant substance found in BOFS is calcium oxide (CaO) followed by iron-containing compounds and silicon dioxide (SiO_2); but, magnesium and manganese oxides are also observed [2, 4]. In a recent study (2019), Wang *et al*. [22] carried out a comprehensive testing regime to evaluate the feasibility of using BOFS powder as a supplementary cementitious material (SCM). The results suggested that BOFS powder shows moderate pozzolanic activity and low hydraulic cement behavior, likely explained by its low amorphous content. BOFS powder contains crystalline calcium silicate phases (*i.e.*, C_3S and C_2S), but these minerals may not necessarily be reactive [22].

In recent years, due to increased environmental concerns and more restrictive regulations regarding the extraction and use of natural aggregates for the concrete industry, the feasibility of using particles as fine aggregate substitutes has been investigated [5-7, 9]. The effects that BOFS have on principal mechanical properties of cementitious materials, following fine aggregate substitutions have been documented. However, there is a paucity of fundamental materials investigations reporting the mechanical effects that impregnating BOFS with heavy metals prior to fine aggregate substitution can have on the hydration of antimicrobial cement-based materials.

In response, this study focuses on the effects that copper (Cu) impregnation can have on the hydration process and mechanical properties of ordinary portland cement (OPC) mortars when these metal-laden slag particles replace 40% of the fine aggregate mass. The 40% percent substitution of fine aggregate by BOFS particles (0.30-0.85 mm grain size) was chosen based on recent investigations by the authors [8-10]. Kinetics of cement hydration in the

presence of Cu-laden BOFS particles were characterized by temporal heat liberation patterns using accepted isothermal calorimetry methods adapted for mortars [23, 24]. Additionally, quantitative X-ray diffraction (QXRD) and electron microprobe analysis (EMPA) were employed to investigate microstructural evolution and to map copper concentrations in sections of cured mortars including Cu-laden BOFS. The following formulations were characterized by weight percent substitution of conventional fine aggregate by mass: Control (0% BOFS), 40% unmodified BOFS substitution, and 40% Cu-laden BOFS substitution. No other admixtures were used in this study. Results from this study provide a framework to leverage metal-laden BOFS particles into a beneficial application for special cementitious material applications.

2. Materials and Methods

2.1 Materials

A bulk cement (Type I/II) manufactured by LafargeHolcim (Florence, CO, USA) that complies with ASTM C150 [25] was used. Chemical and physical characteristics of this cement are shown in **Table 1**. Ottawa sand that conforms to ASTM C778 was obtained from U.S. Silica Company (USA) [26]. Water saturation potential and saturated surface-dry (SSD) bulk specific gravity of Ottawa sand were determined per ASTM C128 [27] and presented in a previous paper by the authors [28] (**Table 2**). Basic oxygen furnace slag (BOFS) was supplied by the Indiana Harbor East Steel Mill complex (Indiana, USA). $Cu(NO_3)_2$ (99% purity, Acros Organics) was utilized to adsorb Cu onto BOFS particles.

Table 1: Chemical and physical properties of OPC cement Type I/II from LafargeHolcim US.

CaO	SiO_2	Al_2O_3	Fe_2O_3	SO_3	MgO	Loss on Ignition (LOI)	Insoluble Residue (IR)	Blaine Fineness (m^2/kg)	C_3S	C_2S	C_3A	C_4AF	$C_3S + 4.75C_3A$
62.2%	19.1%	4.2%	3.2%	3.7%	1.3%	2.50%	0.92%	440	61%	7%	6%	10%	87%

Table 2: Bulk saturated surface dry (SSD) specific gravity, sorption capacity and mass-based sieve analysis of the fine aggregate (Ottawa sand).

			Passing by mass (%) through sieve:					
Fine aggregate	Bulk Saturated Surface Dry (SSD) specific gravity	Water saturation potential (%)	10	20	40	60	100	200

Ottawa sand	2.65	0.81	100.0	100.0	69.50	14.79	2.86	0.03

2.2 Experimental methods

2.2.1 Characterization of BOFS

BOFS particle size distribution was determined as per ASTM D422 [29]. BOFS grain size ranged from 0.30 mm (sieve #50) to 0.85 mm (sieve #20) with a mean grain size (D_{50}) of 0.43 mm. The relative densities (specific gravities for oven-dry (OD) and saturated surface-dry (SSD)) and water sorption for the BOFS were determined per ASTM C128 [27] and presented in **Table 3**.

The equilibrium pH was determined by addition of 1 g of BOFS into 5 mL of deionized (DI) water. The suspension was sparged with N_2 and mixed for 24 h to reach equilibrium prior to pH measurement; the final pH was 12.54. The chemical composition of BOFS particles was determined by X-ray fluorescence (XRF) spectrometry and the results are also listed in **Table 3**.

Table 3: Chemical composition and relative density (specific gravity), bulk density, water sorption, and pH of BOFS.

CaO	**SiO_2**	**Al_2O_3**	**Fe_2O_3**	**SO_3**	**MgO**	**MnO**	**P_2O_5**	**Na_2O**	**Particle specific gravity (OD)**	**Particle specific gravity (SSD)**	**Apparent specific gravity**	**Bulk density (g/cm^3)**	**pH**
37.6%	14.9%	2.5%	22.3%	0.2%	10.6%	5.3%	1.1%	0.1%	3.18	3.27	3.52	1.843	12.5

Mineralogy of the BOFS sample was determined by X-ray powder diffraction (XRD). XRD data were collected by a Siemens D500 X-ray computer-automated diffractometer using Cu Kα X-ray radiation. The sample refraction spectra were observed from 5 to 65 ° (2θ) with a step size of 0.02 ° and a dwell time of 2 seconds per step. BOFS mineral composition shown in **Fig. 1**, was obtained through peak analysis of the XRD diffractogram using Jade software (MDI, Version 9) and the International Centre for Diffraction Data (ICDD) 2003 database.

Major crystalline peaks identified corresponded to: larnite (Ca_2SiO_4); srebrodolskite ($Ca_2Fe_2O_5$); wüestite (FeO); merwinite ($Ca_3Mg(SiO_4)_2$); magnesioferrite ($MgFe_2O_4$); and akermanite ($Ca_2MgSi_2O_7$). The BOFS appears to be far less amorphous than other steel slags (*i.e.*, ground granulated blast furnace slag (GGBFS) and ladle furnace slag (LFS)) [22], as an obvious amorphous hump is not detected [30].

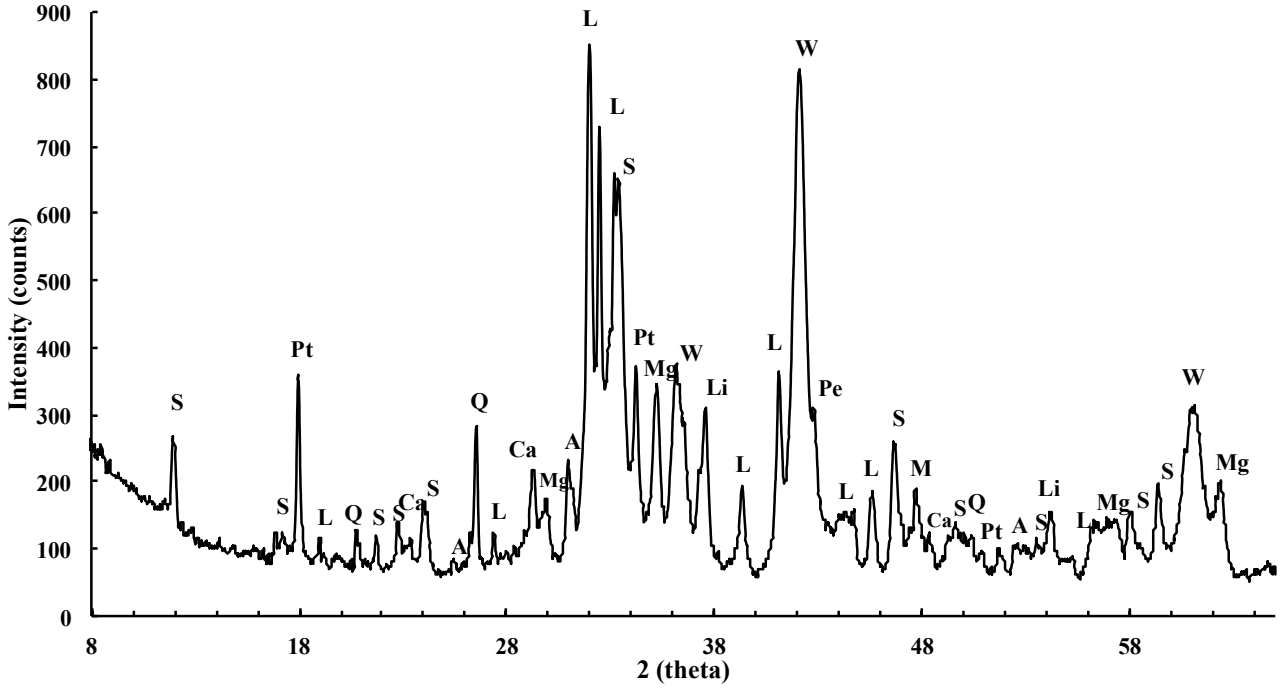

Fig. 1. XRD pattern for BOFS sample (as-received). Major crystalline peaks identified are: larnite (L); srebrodolskite (S); wüstite (W); merwinite (M); magnesioferrite (Mg); akermanite (A); portlandite (Pt); calcite (Ca); lime (Li); and quartz (Q).

2.2.2 Copper (Cu) sorption

To obtain Cu-laden BOFS, the particles were impregnated with soluble metals up to their saturation capacity. The sorption process was performed as follows. First, $Cu(NO_3)_2$ was added to a volume of DI water needed to reach a 12mM Cu concentration. The pH was adjusted to pH 7.6-8.0 to reach an optimum range that favors Cu precipitation as hydroxides using NaOH. Next, BOFS grains were added to this solution in a liquid-to-solid ratio of 20:1 and mixed for 24 h at 150 r/min and room temperature. After this process, the Cu-laden BOFS was

136 separated from the solution by sieving (mesh No. 50), rinsed with DI water, and oven-dried at 40 °C. Sorbed Cu
137 content by these BOFS particles was confirmed by Inductively Coupled Plasma Optical Emission Spectroscopy
138 (ICP-OES) using a calibrated ARL 3410+ and modifications to a widely accepted technique developed by Farrell
139 *et al*. [31]. The Cu detection limit was 42 ppb. The concentration of Cu sorbed onto the BOFS particles surface,
140 normalized by the original BOFS mass, was of 17.9 mg Cu/g BOFS. The two types of BOFS used in this study
141 will be respectively referred to hereafter as BOFS-U (unmodified basic oxygen furnace slag) and BOFS-Cu (Cu-
142 laden basic oxygen furnace slag).

143 **2.2.3 Sample preparation**

144 Three mortar lots were prepared: a Control formulation (not including BOFS) and two formulations where the
145 fine aggregate of these formulations was replaced (by mass) with 40% BOFS as received (BOFS-U) and Cu-laden
146 BOFS (BOFS-Cu) respectively. All formulations were prepared with a water-to-cement (*w/c*) ratio = 0.45 and a
147 sand-to-cement (*s/c*) ratio of 2.1. The water sorption capacity of BOFS particles (*i.e.*, 3.1 %) was considered and
148 included in the mixing water to achieve an effective *w/c* = 0.45. Formulations containing BOFS are labeled
149 according to the following convention: BOFS-Cu-40% denotes a formulation using BOFS particles loaded with
150 Cu (BOFS-Cu) substituting 40% (by mass) of the fine aggregate (Ottawa sand). The formulation containing no
151 BOFS particles was labeled only as "Control." Additionally, one cement paste formulation (*i.e.*, without sand
152 addition) containing BOFS-Cu particles in an equivalent amount to that introduced to the BOFS-Cu-40% mortar
153 formulation, was included for elemental surface-mapping with an electron microprobe analysis (EMPA). All
154 formulations were manually mixed as follows: First, cement was added to the total amount of water and mixed for
155 30 s. Then, the total amount of fine aggregate (Ottawa sand) and BOFS particles (BOFS-U or BOFS-Cu), which
156 were previously dry mixed, were added and mixed for an additional 30 s. After this, formulations were mixed for
157 an additional minute up to a total maximum mixing time of 2 minutes.

158 **2.2.4 Isothermal calorimetry**

159 Heat flow (mW/g) was measured at the U.S. Bureau of Reclamation (USBR-Denver) using a TAM Air 8-Channel
160 standard volume isothermal calorimeter (TA Instruments, USA). The calorimeter included an array of reacting

and non-reacting (control) channels that were capable of eight simultaneous measurements. During this study, the measuring cells within the calorimeter were kept in isothermal conditions (23 ± 0.03 °C). The reference material samples, located in the non-reacting control channels, consisted of 5.5 g of siliceous sand. All observations were collected and reported in duplicate. Freshly mixed cement mortar (5.5 g) was weighed into a 20 mL glass ampoule for each sample. The glass ampoule was sealed and placed into the calorimeter within 5 min after initial mixing, and the heat liberated was continuously monitored and recorded for approximately 118 h. External mixing was applied to ensure complete mixing. For this reason, the initial heat emission after the cement contacted with the mixing water was not measured. As recommended by other calorimetry investigations that include external mixing protocols, the integration of the heat flow accounted for the influence of external mixing energy [23, 32]. In the case of OPC, the first 30 min of hydration contributed less than 6 J/g to the cumulative heat release of the sample [32]. Integration of the heat flow was thus started 30 min after the initial contact of mixing water with cement to enable time for temperature equilibration, as described above. The heat liberated during hydration and the cumulative heat flow was normalized to the cement mass of the respective samples.

2.2.4.1 Calorimetry set times

Initial and final set times were determined based on the first derivative of the heat flow curves according to an identical procedure implemented in the study by Hu, *et al*. (2014) [33]. In this study, the initial set time was defined as the time at which the first derivative curve reaches a maximum, while the final set was defined as the time at which the first derivative equals zero after the initial set time. The first derivatives of heat flow curves (d(q)/d(t)) were obtained from the original heat flow curves.

2.2.5 Compressive strength

After 7, 28, and 240 days of continuous moist curing (temperature 23 ± 2 °C; RH >95%), the compressive strength of triplicate samples was determined as per ASTM C109 [34]. Load was applied to specimens in a calibrated compression press at a load-controlled rate of 1.32 kN/s using an Instron compression test machine.

2.2.6 Quantitative X-ray diffraction (QXRD)

Mineralogy was characterized using specialized software (RockJock®) developed at the United States Geological Survey (USGS) [35]. This software utilizes the measured peak intensities as input data and calculates the abundance (in weight percent) of all identified minerals using internal standards. This software has been recommended by various investigators [36] after comparing it to the Rietveld approach (Topas, Academic), with obtained results within 1 to 2 wt. % of actual mineral abundance values [35, 37].

2.2.6.1 Internal standards

Internal standards for the classic minerals emerging in OPC mortars hydration process were prepared using a modified method introduced by D.D. Ebrel [35], which was adapted to employ corundum (Al_2O_3) and kaolinite (KGa-2) instead of zincite (ZnO). Calcite, portlandite, hydrotalcite, katoite, BOFS, and unhydrated cement were obtained from commercial manufacturers (Sigma-Aldrich and LafargeHolcim, USA), while ettringite and monosulfoaluminate were synthesized in the laboratory following the methods described by Yoon and co-workers [38]. For each internal standard, two samples were prepared: for the first, one gram of the homogenized material was obtained and named "pure sample"; as subsequent standard included one gram of the homogenized material was mixed with 20% corundum and 40 % kaolinite and named "mix sample." All measurements were made with ± 0.00005 g accuracy. Corundum and kaolinite were used to normalize peak heights between samples and align diffraction patterns. Each sample was then ground in a McCrone micronizing mill with 4 mL isopropanol for 5 minutes, generating particle sizes on the order of 10-30 μm. After drying at ambient temperature for 16 h inside a hood, both samples were transferred to a plastic scintillation vial with three acrylic balls (~1 cm in diameter) along with 350μL of Vertrel ® solution (Dupont, USA) and shaken for 5 minutes. The powder of each sample was first passed through a 500 μm sieve (sieve # 35) to break up larger clumps and loaded again in the plastic scintillation vial along with 250 μL of Vertrel ® solution and shaken for another 5 minutes. After this, the powder of each sample was passed through a 250 μm sieve (sieve # 60) to break any clumps and loaded onto a standard XRD holder. For each sample, the corresponding pure and mixed specimen were analyzed using a Siemens D500 X-ray diffractometer from 5 to 65 ° 2θ, using Cu Kα X-ray radiation, with a step size of 0.02 ° and a dwell time of 2 s per step. Internal standard XRD patterns are shown in **Supplementary Information.**

2.2.6.2 Mortar sample preparation for QXRD

The following formulations were prepared for QXRD: Control (0% BOFS), BOFS-Cu-40%, and BOFS-U-40%. Five samples of each formulation were cast in separate plastic dishes (2.5 cm in diameter) and placed in a moist chamber (23 ± 2 °C; RH >95%) until the designed age of test: 1, 3, 7, 28 and 240 days. At the defined age, one of the mortar samples was removed from the moist curing chamber, and the hydration process stopped by crushing it into a powder with an agate mortar and pestle in 6 mL of isopropanol ($(CH_3)_2CHOH$). The resulting slurry was emptied into a glass vial and left to dry for 24 h at ambient temperature. Once it reached a dry condition, the air inside the glass vial was replaced with pure nitrogen gas. Then, the vial was immediately capped. The resulting powder was prepared for QXRD analysis as follows: 0.8000 g of the mortar powder was mixed with 0.2000 g of corundum to obtain 1.0000 g of homogenized material, where all measurements were made with ± 0.00005 g accuracy. The sample was then ground and prepared following the same procedure described above in order to develope the appropriate internal standard. Once the powder was loaded onto a standard XRD holder, it was also analyzed using a Siemens D500 X-ray diffractometer from 5 to 65° 2θ using Cu Kα X-ray radiation, with a step size of 0.02° and a dwell time of 2 s per step.

2.2.7 Electron microprobe analysis (EMPA)

2.2.7.1 Sample preparation

Cement paste containing BOFS-Cu was cast in a circular plastic mold of 15 mm diameter and 10 mm height. The sample was de-molded after 24 h and cured in moist conditions for 30 days. After that time, the sample was dried in a desiccator for one week. The sample was then polished and prepared following the methodology previously described by Justo-Reinoso and co-workers [19]. After the sample was polished, it was embedded in an epoxy disc of 25 mm diameter and 15 mm in height for EMPA analysis

2.2.7.2 EMPA elemental composition mapping

In order to estimate the distribution of selected elements in the cement paste formulations containing BOFS-Cu particles, four wavelength dispersive spectrometry (WDS) elemental composition maps of Cu Kα, Ca Kα, Al Kα, and S Kα were acquired. The EMPA data acquisition was performed on a JEOL JXA-8230 electron microprobe

outfitted with EDS and WDS attachments. The sample was carbon-coated (ca. 15 nm thin-film) using an Edwards Auto306 dual coater to ensure identical conductivity and analytical conditions with accepted standards. Backscattered Electron (BSE) images were also obtained using the JEOL JXA-8230. The EMPA system was set at 15 keV accelerating voltage, 40nA beam current, and 1 μm beam diameter. The WDS element maps were acquired using an accelerating voltage of 15 keV and a 100nA beam current. The electron beam was defocused between 5 μm and 6 μm to match the pixel size of the maps. A per-pixel dwell time of 10 msec was used. Prior to the acquisition, each spectrometer was calibrated on a series of Astimex standard reference materials. The standards were as follows: Cu: chalcopyrite; Ca: plagioclase; Al: almandine garnet; and S: anhydrite. The Ca Kα, Al Kα, and S Kα maps were obtained using spectrometers equipped with large-area pentaerythritol (PET) monochromaters. The Cu Kα map was obtained using a spectrometer equipped with a large area lithium fluoride monochromater. The energy dispersive X-ray spectra (EDS) were acquired at 15 keV accelerating voltage and accumulated over a 30-sec interval. Results expressed as net counts are semi-quantitative, since each pixel may represent a mixture of two or more mineral phases.

3. Results

3.1 Isothermal calorimetry

Fig. 2 summarizes the rate of heat liberated from cement hydration and the cumulative heat obtained from the following mortar formulations: a Control formulation (0% BOFS) and two formulations where the fine aggregate was substituted (by mass) with 40% BOFS particles, either BOFS-U or BOFS-Cu. For clarity, the heat flow results are presented for the first 30 h of curing, while the cumulative heat curves are presented for a 118-hour observation period.

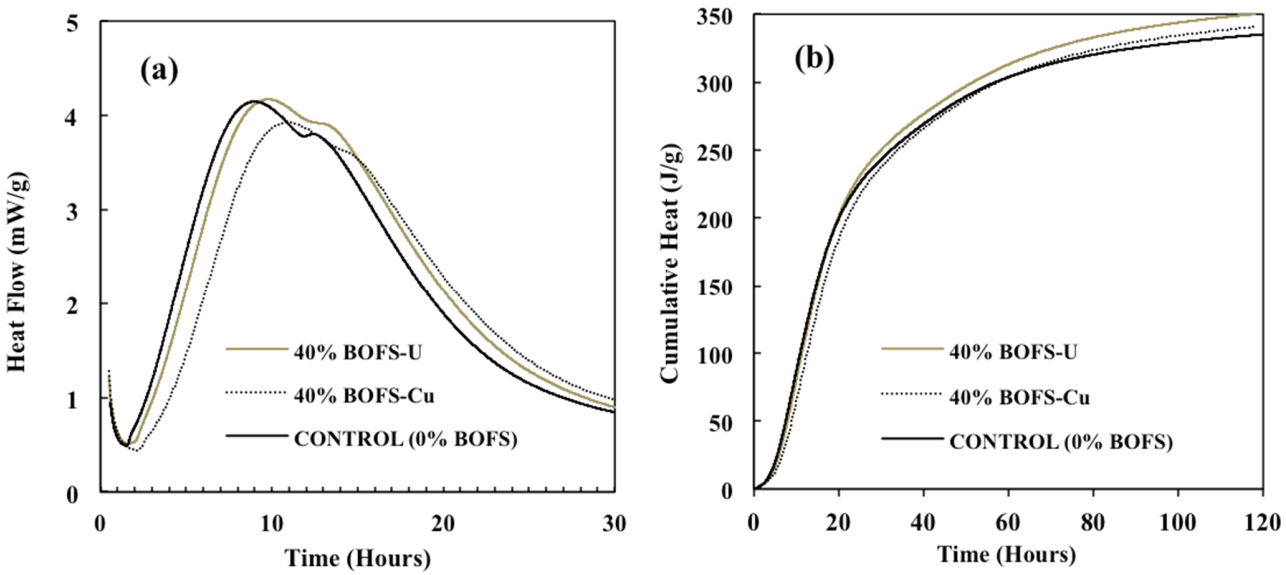

257

258 **Fig. 2: (a)** Heat flow (mW/g) and **(b)** cumulative heat (J/g) for the following cement mortar formulations:
259 Control (0% BOFS), BOFS-U-40%, and BOFS-Cu-40%. Each curve represents the mean value of two
260 measurements.

261

262 The thermal power curve for all the three formulations shows a trace typically associated with the hydration
263 kinetics of hydraulic cementitious mixtures, where a shoulder appears following the primary peak. The primary
264 peak corresponds to the sulfate depletion point, followed by an accelerated calcium aluminate activity peak [23,
265 39]. Following initial dormancy, an acceleration period occurred at 1.6 h for the Control formulation (0% BOFS),
266 while this acceleration was measurably delayed to 1.9 and 2.3 for formulations containing 40% BOFS-U or
267 BOFS-Cu, respectively. In a recent study, a similar delay was observed by Wang *et al.* when they compared the
268 heat flow of an OPC paste to a BOFS paste, where BOFS powder was used as the cementitious material [22]. A
269 main peak followed this acceleration period at 9.0 and 9.8 h for the Control and BOFS-U-40% formulations,
270 respectively. However this peak was delayed (*i.e.*, 10.9 h) for the formulation containing Cu-laden BOFS particles
271 (BOFS-Cu-40%). Further, the height of the main peak (maximum heat rate peak) was decreased slightly when Cu
272 was present. It is well known that the presence of metals may selectively delay cement hydration reactions due to
273 the reduction of the permeability of cement grains likely caused by the rapid chemical precipitation of insoluble

metal hydroxides on their surface [19, 40-42]. Additionally, the conversion of metal hydroxides to metal hydroxyl-species consumes Ca^{2+} and hydroxide ions, and this consumption would, in effect, also delay the supersaturation of the cement pore water and, as a result, the precipitation of C-S-H and portlandite [43].

In **Fig. 2b**, the cumulative heats for the three formulations are presented. These data show that when fine aggregate was replaced by 40% Cu-laden BOFS particles, the heat flow behavior was delayed during the first 63 h, compared to the Control formulation (0% BOFS). After that time, the heat flow curve of the BOFS-Cu-40% formulation behaved similarly to the Control, where both formulations plateau at a similar level (340 J/g) after the testing period (118 h). In contrast, when Cu-free BOFS particles (BOFS-U) were used to replace that same amount of fine aggregate (40% by mass), the heat flow curve is not distinguishable from the Control formulation during the first 19.5 h; after this however, heat evolution from the BOFS-U-40% begins to accelerate and ends up achieving a slightly higher heat flow (350 J/g) than the other two formulations (Control and BOFS-Cu-40%).

A higher cumulative heat response was expected as a result of replacing inert fine aggregate (*i.e.*, sand) with BOFS particles, this due to the pozzolanic properties of the latter [30, 44]. However, the inclusion of these BOFS particles in this study exhibited only a slight difference in the hydration responses, likely, as mentioned by Wang *et al*. [22], by the low amorphous content and presence of some non-reactive crystalline phases of BOFS.

The initial and final set times were obtained from the first derivative of the heat flow curves (**Fig. 3**). As mentioned by Hu *et al.*, longer setting times have been observed from calorimetry methods when compared to ASTM penetration tests in similar cement mortar formulations due to different mechanisms and test configurations [33]. The results indicated that replacement of 40% (by mass) of fine aggregate with either BOFS-U or BOFS-Cu particles, delayed the initial set time of these formulations by 18% and 47%, respectively. Likewise, final set times were delayed 9% and 21% for formulations containing BOFS-U or BOFS-Cu, respectively. These delays were anticipated as the presence of calcium aluminates in BOFS particles are known to react in contact with water, releasing aluminum ions which may be adsorbed on calcium silicate surfaces, thereby likely retarding silicate dissolution and cement hydration [22].

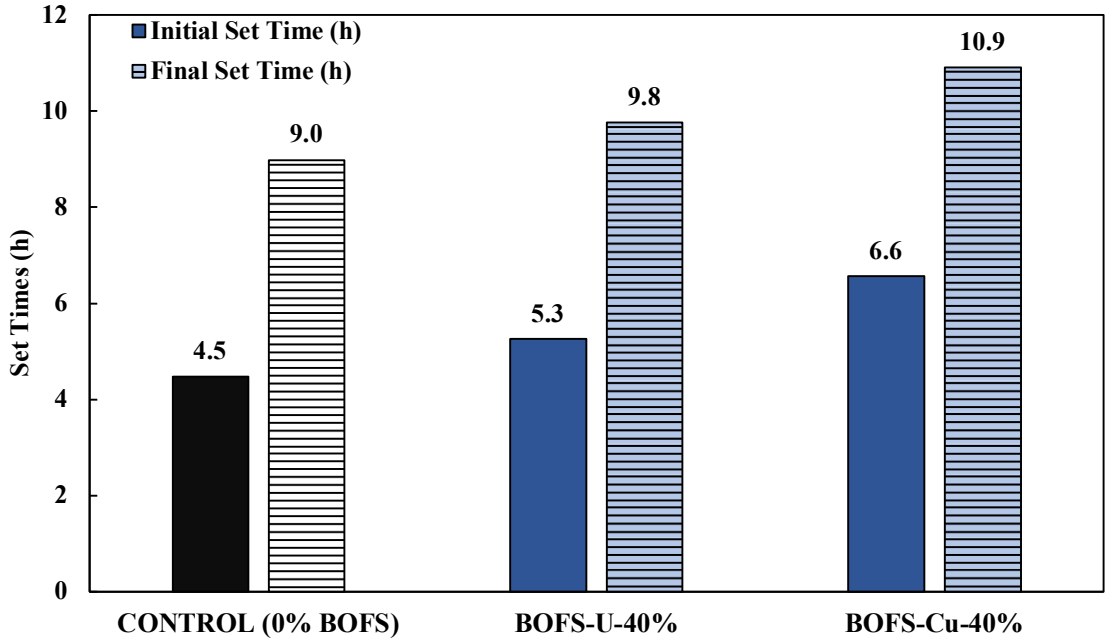

298

299 **Fig. 3**: Initial and final set times calculated from the first derivative of the heat flow curves. (For the first
300 derivative curves see **Supplementary Information**)

301

302 **3.2 Compressive strength**

303 Data suggest that the substitution of 40% (by mass) of the fine aggregate with similarly sized BOFS particles,
304 regardless the presence or absence of Cu, have no significant effect on the compressive strength response when
305 compared to a Control formulation (0% BOFS) after curing times of 240 days (**Fig. 4**). Results were compared
306 using analysis of variance (ANOVA). The results corresponding to the use of Cu-free BOFS-U particles are in
307 accordance with those obtained by other authors in the same percentage replacement range [6, 7, 9, 45]; they
308 reported that cement mortars made with a blend of metal-free BOFS particles (with an average particle size
309 between 0.3 – 0.6 mm) and river sand had comparable compressive strength results to cementitious materials
310 made with only river sand. Likewise, the results regarding BOFS-Cu replacements are in agreement with other
311 authors studying the effect of Cu on the compressive strength of cement mortars after 28-days of curing [9, 46].

312

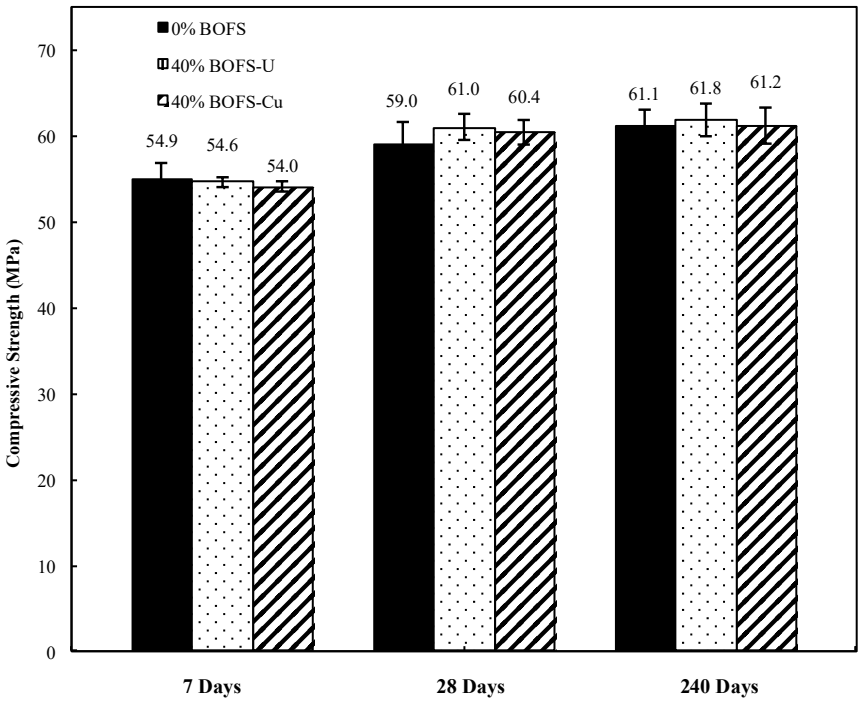

Fig. 4: Influence of the replacement of 40% (by mass) fine aggregate by BOFS (without and with Cu) on compressive strength after a curing period of 7, 28, and 240 days. Results represent the average of three cubic specimens for the following formulations: BOFS-0% (Control), BOFS-U-40%, and BOFS-Cu-40%. Error bars represent ± one standard deviation.

3.3 QXRD

No significant mineralogical differences between the BOFS-U-40% and the BOFS-Cu-40% were observed at the different curing ages investigated in this study (see **Supplementary Information**). QXRD results comparison between Control and BOFS-Cu-40% formulations is shown in **Table 4**. Data suggest a significantly higher content of calcium silicate hydrate (C-S-H) phases and calcite (likely due to carbonation) through the different testing ages for the BOFS-Cu-40% formulation. Lower amounts of quartz were anticipated, since the BOF-Cu-40% formulation replaces 40% of the sand by BOFS.

Table 4: QXRD results comparison between the Control formulation (0% BOFS) and the formulation with 40% fine aggregate replacement (by mass) with BOFS-Cu. Results are shown as weight percentage of the total sample.

	BOF-0% (Control)					BOFS-Cu-40%				
	1-day (wt.%)	3-days (wt.%)	7-days (wt.%)	28-days (wt.%)	240-days (wt.%)	1-day (wt.%)	3-days (wt.%)	7-days (wt.%)	28-days (wt.%)	240-days (wt.%)
Quartz	67.76	66.37	70.08	73.33	71.50	31.96	35.54	33.41	33.20	33.60
Calcite	0.77	0.26	1.09	0.60	0.74	5.69	2.81	2.46	4.82	4.29
Ettringite	0.00	1.38	0.95	0.83	0.93	0.95	0.42	0.79	1.56	1.22
Cement	19.84	13.28	13.23	8.86	8.50	20.70	10.56	6.42	7.45	6.82
BOFS	0.00	0.00	0.00	0.00	0.00	23.65	25.17	26.99	22.50	23.23
Portlandite	3.37	3.99	5.25	4.17	4.93	1.83	3.08	3.40	2.81	3.51
CSH estimate	8.26	14.72	9.40	12.21	13.40	15.20	22.42	26.53	27.66	27.33
TOTAL	100.00	100.00	100.00	100.00	100.00	100.00	100.00	100.00	100.00	100.00

Fig. 5 shows the XRD diffractograms obtained for the Control (0% BOFS) and BOFS-Cu-40% formulations, after 240 days of curing (for XRD diffractograms at other curing ages; see **Supplementary Information**). Quartz, portlandite, ettringite, calcite, and hydrotalcite are present among other hydration products. At the five different ages tested, the diffractograms of both formulations presented similar peaks, with some of these peaks varying in intensity among both formulations.

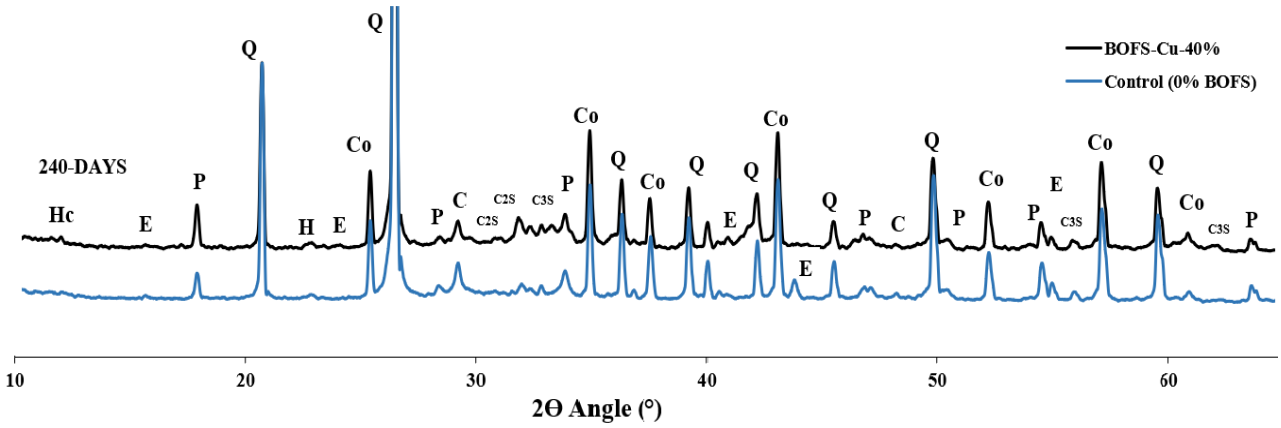

Figure 5: XRD diffractograms for mortar samples with Cu-laden BOFS replacement percentages (by weight) of 0% (Control) and 40% after a moist curing time of 240 days. Hc: hemicarbonate, H: hydrotalcite, E: ettringite, P:

340 portlandite, Q: quartz, C: calcite, C_3S: alite, C_2S: belite, and Co: corundum. See **Supplementary Information** for
341 XRD diffractograms at other curing ages.

342
343
344
345 **3.4 Electron microprobe analysis (EMPA)**

346 Wavelength dispersive spectroscopy (WDS) elemental mapping with energy dispersive X-rays spectroscopy
347 (EDS) was used to assess the proximity of copper (Cu) to the BOFS particles, as well as the distribution of Ca, Al,
348 and S throughout the cement matrix. The WDS elemental map of Cu is shown in **Fig. 6**. The BSE image in **Fig.**
349 **6a** shows the heterogeneity of BOFS particles, and their location overlaid on an elemental Cu concentration map.
350 The EMPA maps show that Cu is concentrated in the BOFS particles but also revealed Cu micro-concentration
351 gradient surrounding the impregnated BOFS particles, above the method detection limit (8 ppm). Microcracks
352 observed in the sample resulted likely from the drying and polishing process prior to encapsulating it in epoxy
353 [47, 48].

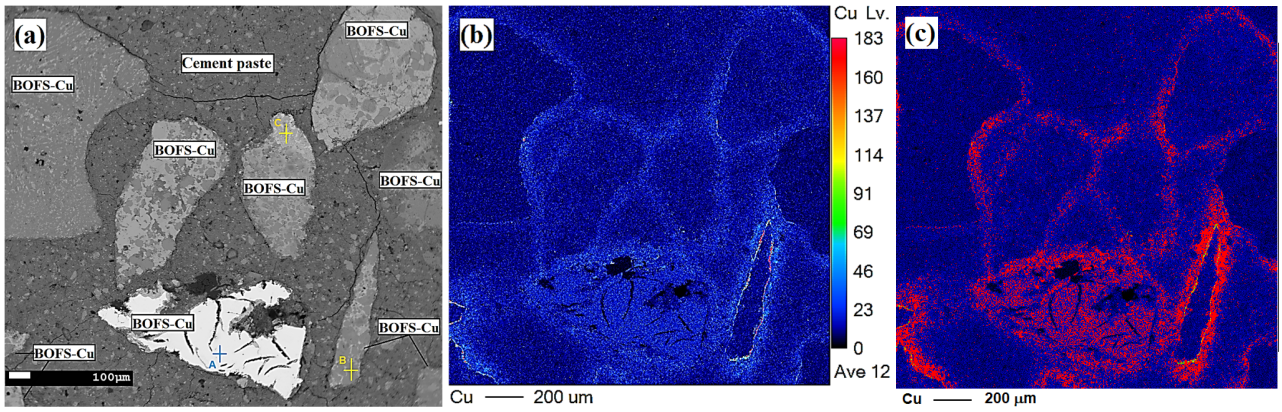

354

355 **Figure 6: (a)** BSE image of the cement paste containing BOFS-Cu is shown with the location points where
356 energy dispersive X-ray spectra (EDS) were obtained; **(b)** WDS elemental mapping of Cu; **(c)** Segmentation
357 decomposition counts ranged between 20 and 80 relative to the Cu WDS elemental map.

358 WDS Cu elemental map is presented in **Fig. 6b**, and a segmentation decomposition image focusing on the
359 proximity of Cu to BOFS particles is shown in **Fig. 6c**. Copper was predominantly limited to a spherical region
360 (~100 µm region) surrounding the BOFS particles. However, some BOFS particles presented significantly higher

levels of Cu than others—either in their close proximity or directly sorbed throughout its surface— likely resulting from the distinct mineralogical composition among these particles. These mineral composition differences might have probably resulted in different sorption and attachment mechanisms of copper onto the BOFS particles surfaces. The WDS elemental maps for calcium (Ca), aluminum (Al), and sulfur (S) in **Fig. 7;** these maps confirm the polymorphic composition of the different BOFS particles within the sample, with some BOFS particles containing higher calcium concentrations than others; still other BOFS particles appear to contain no calcium above the method detection limit. Likewise, BOFS grains presented among them unrelated concentrations of Al. Sulfur was uniformly distributed within the cement matrix and was not associated with the mineralogical composition of the BOFS particles.

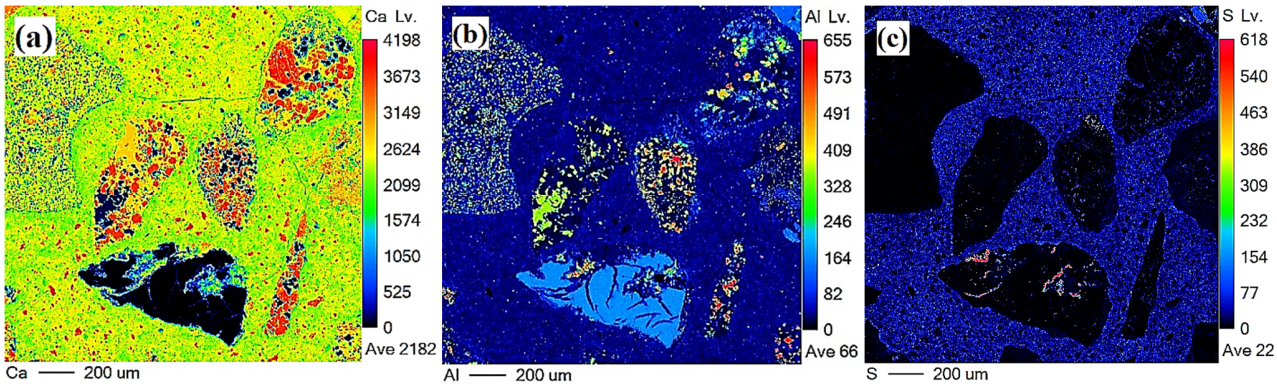

Figure 7: WDS elemental mapping of the cement paste containing Cu-laden BOFS. **(a)** calcium (Ca); **(b)** aluminum (Al); and **(c)** sulfur (S); Color scale is proportional to the mass concentration of each element relative to its highest detected concentration.

Three EDS spectra were obtained from BOFS particles with significantly different Cu mobilization responses (**Fig. 8**). The location points of these EDS are shown in the BSE image (**Fig. 6a**). Point A corresponds to a BOFS grain with a high content of iron (Fe) (51.3 Atom %); point B to a BOFS grain with a predominant chemical composition of Ca and Al (26.3% and 17.2 Atom %, respectively); while point C shows a significant presence of Ca in combination with silicon (Si) (28.9% and 14.1 Atom %, respectively). The peaks of carbon (C) were

expected in all the EDS spectra as a result of the sample coating process with carbon. The EDS points were located inside BOFS particles where Cu presence is almost negligible, which is the reason for little to no evidence of Cu peaks.

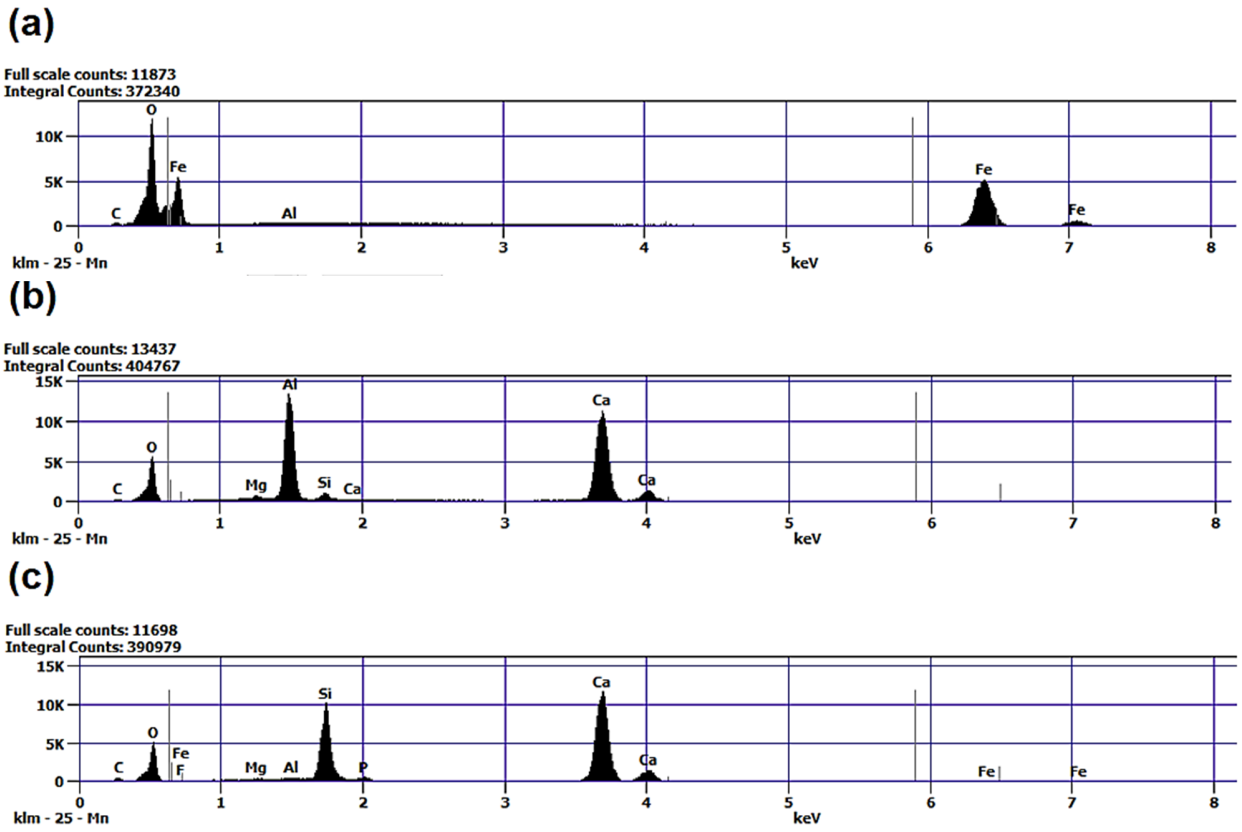

Figure 8: Energy dispersive x-rays spectra (EDS), obtained from a cement paste containing Cu-laden BOF-S particles, are shown for three different BOFS particles: **(a)** higher density particle; **(b)** particle with significant Cu concentration surrounding it, and **(c)** ordinary BOFS particle. The locations of EDS points are shown in **Fig. 6(a)**.

4. Discussion

4.1 Isothermal calorimetry

Concerning the BOFS-U-40% formulation, heat flow curve results suggest that cement hydration is slightly delayed during the first 18 h of the process, and then accelerated when compared to the Control formulation. The

399 delay could be associated with the presence of some minor elements on BOFS surfaces, which may dissolve in the
400 pore solution and affect the cement hydration process. Aluminum ions released from BOFS particles may be
401 adsorbed on calcium silicate surfaces, thereby delaying silicate dissolution [22]. Moreover, Mn [49, 50] and Mg
402 [2, 51], also present in BOFS particles, are two elements know to retard cement hydration; this could be
403 compounded by the chemisorption of Ca^{2+} ions onto the BOFS surface. Here, BOFS particle surfaces may act as a
404 calcium sink, where Ca^{2+} ions in the pore solution may be coordinated by the aluminum associated with BOFS
405 particles (**Fig. 7**) similar to mechanism observed on the surfaces of aluminum-abundant fly ashes [52]. When
406 compared to the Control formulation, the higher cumulative heat liberated from this formulation (BOSF-U-40%),
407 from 18 h onwards, is likely associated to the reaction of active minerals (C_3S and C_2S) that are present on BOFS
408 particles' surfaces with alkali hydroxides and calcium hydroxides (**Fig. 9**) [22, 53]. Regarding this aspect, Yuji
409 [54] observed that small fibrous C-S-H crystals were able to grow from steel slag particles when these were used
410 to replace fine aggregate in concrete samples. Guo *et al.* [7] also replaced a fraction of the fine aggregate by steel
411 slag particles in normal-strength concrete specimens. They observed slight effects on the mechanical properties
412 attributable to the presence of active C_2S and C_3S (on steel slag particles) participating in the hydration process.
413 As a result of these fine aggregate replacements, BOFS particles can contribute to the heat of hydration
414 (pozzolanic activity) in a sustained way that inert sand particles cannot.

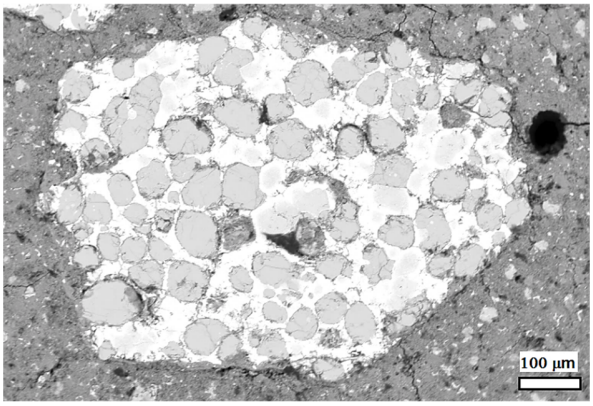

415

416 **Figure 9**: BOFS particle with rounded belite (C_2S) crystals.

417

418 Replacing 40% (by mass) of the fine aggregate with Cu-laden BOFS particles resulted in a delay of the cement
419 hydration during the first 63 h, after that, it showed a modest, but steady increase when compared to the Control
420 formulation. This initial delay could be explained as a result of the Cu sorbed onto the BOFS particles. Several
421 authors [40, 41, 55, 56] agree that the presence of heavy metals may selectively delay cement hydration reactions
422 due to a reduction of the permeability of cement grains. On the other hand, the acceleration observed after an
423 initial delay may be associated with the reaction of active minerals (C_3S and C_2S) that form part of the mineral
424 composition of BOFS particles. When BOFS particles get in contact with water, they react with sodium and
425 potassium alkali and calcium hydroxides to produce additional CSH. However, it should be noted that this
426 reaction, due to the calcium silicates present in steel slag, is more reduced than that in portland cement because
427 the cooling rate of steel slag is much lower than that of portland cement (pozzolanic reaction) [57, 58].

428 In summary, comparing the cumulative heat released after 118 h of curing in **Fig 2b**, the presence of BOFS-U
429 particles (without Cu) induces an acceleration in the hydration process when compared to its Control formulation.
430 In contrast, the presence of Cu in the BOFS induced an initial delay that later compensated to achieve a similar
431 cumulative heat value as the Control formulation.

432 **4.2 QXRD**

433 It is well known that the production process of BOFS can influence the reactivity of the final proportions of its
434 calcium silicates [2, 57]. BOFS particles used in this study were rapidly quenched, resulting in more reactive
435 calcium silicate. Relatively higher calcite and C-S-H contents were observed during the curing of the
436 formulations containing 40% BOFS replacements. Higher C-S-H contents were expected, as different authors
437 have observed that most silicate and aluminate in steel slag particles used as fine aggregates can hydrate
438 producing additional C-S-H, C-A-S-H, and portlandite after 90 days of reaction [54, 57]. After the initial addition
439 of water, hydration of BOFS in the presence of OPC depends largely upon breakdown and dissolution of the
440 vitreous slag structure by hydroxyl ions that are liberated during the hydration of OPC [44]. The increase in pH of
441 the supersaturated solution elevates silica dissolution of aluminosilicates present in the BOFS [59, 60]. Moreover,
442 it has been shown that percentage of soluble silica from slag is almost doubled when pH increases from 13 to 14

443 in the solution [59]. Wang also observed that a significantly small instant reaction takes place when the slag is
444 initially mixed with water, preferentially releasing Ca^{2+} and Al^{3+} ions to the solution. However, the reaction is
445 limited until more alkali, calcium hydroxide (portlandite), and sulfates are available for additional reactions [44].
446 Consequently, as a result of these hydration reactions, BOFS particles are able to react with the alkali and
447 portlandite present in the solution to produce additional C-S-H and C-A-S-H [44]. Additionally, the calcium,
448 which exists as various forms of compounds in BOFS, provided the potential for carbonation when exposed to
449 atmospheric CO_2 during the storage period [61], likely resulting in the higher calcite contents observed for BOFS
450 formulations. Portlandite was observed in slightly lower percentages in BOFS-U-40% when compared to Control.
451 However, these differences are likely the result of the pozzolanic effect of BOFS particles related to the presence
452 of the SiO_2 merwinite phase, as mentioned by Muhmood *et al*. [62].

453 **4.3 EMPA elemental mapping**

454 The highest Cu levels remained in near the interface of BOFS particles with the bulk cement paste; however, it
455 was evident that some BOFS particles presented significantly higher Cu associations than others (**Fig. 6c**).
456 Furthermore, it is evident that some of the Cu that was originally sorbed onto BOFS particle surfaces experienced
457 some degree of mobilization that resulted in copper dispersion into the cement matrix, albeit at levels near the
458 detection limit of elemental mapping. Even though Cu diffusion away from the BOFS particles was relatively
459 small, this Cu may be at a level and distribution which influences the early cement hydration process according to
460 calorimetry results previously discussed.

461 In **Fig. 6a**, the heterogeneity of the BOFS particles in mineralogical composition can be readily observed. Here,
462 BOFS particles containing heavier elements (*e.g.*, Fe) appear in lighter shades of gray, while minerals containing
463 only lighter elements (Ca, Al, Si) appear in darker shades. These variations were also corroborated through EDS
464 spectra obtained from three different BOFS particles (**Fig. 8**). As has been observed by several authors, even
465 BOFS particles coming from the same furnace source can have heterogeneous chemical compositions [6], and this
466 variability could explain the differences in Cu levels observed among BOFS particles in this study. Moreover,

previous studies with commercial activated carbon, analogously impregnated with copper and added to OPC mortar formulations, revealed homogeneous metal distributions in and near these carbonaceous particles [19]. These results suggest that variations in chemical composition of the BOFS particles observed here, are responsible for the variance in copper associations with these fine aggregate substitutes. Different studies have shown a strong binding capacity of Fe-rich particles, mainly containing Fe_3O_4 and Fe_2O_3, for Cu^{2+} ions [63-65]. The mechanisms responsible for binding these Cu^{2+} ions are adsorption and precipitation, being the latter the principal mechanism when BOFS particles are used as a result of the dissolution of the hydroxides present in their surfaces [63, 64]. Cu^{2+} ions electronegativity form very strong covalent bonds with the oxygen atoms present in iron oxides [64], which along with the acid-neutralizing ability of these BOFS particles, allows Cu^{2+} ions to remain firmly attached to these particles [66]. Regarding the effects that the alkaline environment during OPC hydration process may have on these attached Cu^{2+} ions, Tamez *et al.* observed that no significant reduction in the binding of these Cu^{2+} ions to iron oxides was observed in the presence of a solution consisting of a combination of cations normally present in the pore solution (Na^+, K^+, Mg^{2+}, and Ca^{2+}) [65].

5. Conclusions and significant findings

The antimicrobial effect resulting from Cu-laden BOFS particles in OPC cement mortars has been documented as an effective, potentially low-cost, long-term alternative [8]. This study provides valuable insights on the use of these biocidal particles, with respect to the potential for Cu mobilization within cement matrix, as well as the effects that these antimicrobial aggregates may have on the hydration process and mechanical properties of cementitious materials, and, in this way, expand mechanistic knowledge of materials designed to counter microbially-induced concrete corrosion.

The following statements highlight the conclusions and significant findings of this work:

- No significant differences were observed on the compressive strength behavior between formulations containing BOFS particles regardless of the presence or absence of Cu when these BOFS particles were used as partial replacements (40% by mass) of fine aggregate in similar mortar formulations.
- The use of 40% replacement percentage of BOFS particles (BOFS-U or BOFS-Cu) increased the conventional dormant period of the cement hydration process, resulting in higher setting times for these formulations. The formulation containing Cu-laden BOFS particles experienced an expected delay in these setting times when compared to the other formulations.
- The replacement of 40% fine aggregate (by mass) with Cu-free BOFS particles (BOFS-U) accelerated the hydration process after 18 h when compared to Control formulation, resulting in higher cumulative heat liberation at the end of the testing period (118 h). This acceleration is likely originated by the reaction of active minerals (C_3S and C_2S) present in BOFS particles. On the other hand, formulations containing Cu-laden BOFS particles (BOFS-Cu) experienced an initial delay related to the presence of Cu that was later overcome to reach a similar cumulative heat as the one observed for the Control formulation, indicating that a similar degree of hydration was achieved after 118 h.
- Relatively higher C-S-H contents were observed during the curing of the formulations containing 40% BOFS replacements, which was likely the result of the additional hydration of calcium silicates present on BOFS particle surfaces and pozzolanic activity.
- Although at trace levels, Cu was detectable throughout the cement matrix even though BOFS was the only Cu source, indicating that some Cu desorbed from non-Fe-rich BOFS particles during cement hydration. Even in the presence of extremely high concentrations of alkali cations (Na^+, K^+, Ca^{2+}, and Mg^{2+}), there is a strong affinity of Cu^{2+} ions to iron oxides (i.e., Fe_2O_3) present in these Fe-rich BOFS particles [65]. Nevertheless, when Cu was slightly desorbed, it was predominately limited to the immediate vicinity surrounding BOFS particles (~100 μm). It is observed that these Cu levels significantly varied among BOFS particles due to their heterogeneous chemical nature. This finding implies the need for controlling the homogeneous spatial distribution of these BOFS particles to obtain the desired antimicrobial effects.

Declaration of competing interest

The authors have no conflicts of interest in conducting and reporting this research. All funding sources have been adequately identified, acknowledged, and included in the text. This work is neither published nor under consideration elsewhere.

Acknowledgments

The authors gratefully acknowledge Catherine Lucero of the Bureau of Reclamation (USBR-Denver), Dr. Kate Campbell and Dr. Tyler Kane of the United States Geological Survey (USGS-Boulder), and Dr. Aaron Bell, electron microprobe laboratory manager at the University of Colorado-Boulder, for their support and insights with isothermal calorimetry, XRD, and EMPA tests respectively. This research was partially supported by the Mexican National Council for Science and Technology (CONACYT) through the Fellowship No.103259 and by the Department of Civil, Environmental & Architectural Engineering at the University of Colorado-Boulder through a Doctoral Assistantship for Completion of Dissertation. This work represents the views of the authors and not necessarily those of the sponsors.

References

1. Association, W.S., *Steel Statistical Yearbook 2019- Concise version*. 2019: Brussels, Belgium. p. 46.
2. Naidu, T.S., C.M. Sheridan, and L.D. van Dyk, *Basic oxygen furnace slag: Review of current and potential uses.* Minerals Engineering, 2020. **149**: p. 106234.
3. Kumar, D.S., et al., *Measurement of metallic iron in steel making slags.* Measurement, 2019. **131**: p. 156-161.
4. Yi, H., et al., *An overview of utilization of steel slag.* Procedia Environmental Sciences, 2012. **16**: p. 791-801.

5. Ding, Y.-C., et al., *Study on the treatment of BOF slag to replace fine aggregate in concrete.* Construction and Building Materials, 2017. **146**: p. 644-651.
6. Bodor, M., et al., *Laboratory investigation of carbonated BOF slag used as partial replacement of natural aggregate in cement mortars.* Cement and Concrete Composites, 2016. **65**: p. 55-66.
7. Guo, Y., et al., *Utilization of unprocessed steel slag as fine aggregate in normal-and high-strength concrete.* Construction and Building Materials, 2019. **204**: p. 41-49.
8. Caicedo-Ramirez, A., *Doctoral Thesis: Antimicrobial Aggregates for the In-Situ Control of Microbially Induced Concrete Corrosion*, in *Department of Civil, Environmental, and Architectural Engineering*. 2018, PhD Thesis University of Colorado-Boulder: Boulder, Colorado (USA).
9. Justo-Reinoso, I. and M.T. Hernandez, *Use of Sustainable Antimicrobial Aggregates for the In-Situ Inhibition of Biogenic Corrosion on Concrete Sewer Pipes.* MRS Advances, 2019. **4**(54): p. 2939-2949.
10. Justo-Reinoso, I.A., *Microstructural Responses of Cementitious Materials to Substitutions with Fine Antimicrobial Aggregates*, in *Civil, Environmental, and Architectural Engineering (CEAE)*. 2020, University of Colorado-Boulder: Boulder, CO, USA.
11. Grengg, C., et al., *Advances in concrete materials for sewer systems affected by microbial induced concrete corrosion: A review.* Water research, 2018. **134**: p. 341-352.
12. Jia, R., et al., *Microbiologically influenced corrosion and current mitigation strategies: a state of the art review.* International biodeterioration & biodegradation, 2019. **137**: p. 42-58.
13. Noeiaghaei, T., et al., *Biogenic deterioration of concrete and its mitigation technologies.* Construction and Building Materials, 2017. **149**: p. 575-586.
14. Wu, M., et al., *Microbiologically induced corrosion of concrete in sewer structures: A review of the mechanisms and phenomena.* Construction and Building Materials, 2020. **239**: p. 117813.
15. Caicedo-Ramirez, A., A.L. Ling, and M. Hernandez, *Diffusion susceptibility demonstrates relative inhibition potential of sorbent-immobilized heavy metals against sulfur oxidizing acidophiles.* Journal of microbiological methods, 2016. **131**: p. 42-44.

16. Vincke, E., N. Boon, and W. Verstraete, *Analysis of the microbial communities on corroded concrete sewer pipes–a case study.* Applied Microbiology and Biotechnology, 2001. **57**(5-6): p. 776-785.
17. Haile, T. and G. Nakhla, *The inhibitory effect of antimicrobial zeolite on the biofilm of Acidithiobacillus thiooxidans.* Biodegradation, 2010. **21**(1): p. 123.
18. Haile, T. and G. Nakhla, *A novel zeolite coating for protection of concrete sewers from biological sulfuric acid attack.* Geomicrobiology Journal, 2008. **25**(6): p. 322-331.
19. Justo-Reinoso, I., et al., *Dispersion and Effects of Metal Impregnated Granular Activated Carbon Particles on the Hydration of Antimicrobial Mortars.* Cement and Concrete Composites, 2020. **Volume 110**: p. 103588.
20. Justo-Reinoso, I., et al., *Fine aggregate substitution with acidified granular activated carbon influences fresh-state and mechanical properties of ordinary Portland cement mortars.* Construction and Building Materials, 2019. **207**: p. 59-69.
21. Teir, S., et al., *Dissolution of steelmaking slags in acetic acid for precipitated calcium carbonate production.* Energy, 2007. **32**(4): p. 528-539.
22. Wang, Y. and P. Suraneni, *Experimental methods to determine the feasibility of steel slags as supplementary cementitious materials.* Construction and Building Materials, 2019. **204**: p. 458-467.
23. Scrivener, K., R. Snellings, and B. Lothenbach, *A Practical Guide to Microstructural Analysis of Cementitious Materials*. 2016, FL (USA): CRC Press. 540.
24. Wadsö, L., *Applications of an eight-channel isothermal conduction calorimeter for cement hydration studies.* Cement international, 2005(5): p. 94-101.
25. ASTM, *C150/C150M-18 Standard Specification for Portland Cement*. 2018, ASTM: West Conshohocken, PA, 19428, United States. p. 10.
26. ASTM, *C778-17 Standard Specification for Standard Sand*. 2017, ASTM: West Conshohocken, PA, 19428, United States. p. 3.
27. ASTM, *C128-15 Standard Test Method for Relative Density (Specific Gravity) and Absorption of Fine Aggregate*. 2015, ASTM: West Conshohocken, PA, 19428, United States. p. 6.

28. Justo-Reinoso, I., et al., *Fine aggregate substitution by granular activated carbon can improve physical and mechanical properties of cement mortars.* Construction and Building Materials, 2018. **164**: p. 750-759.
29. ASTM, *D422 Standard Test Method for Particle-Size Analysis of Soils*. 2014, ASTM: West Conshohocken, PA, 19428, United States. p. 8.
30. Guo, H., et al., *Iron recovery and active residue production from basic oxygen furnace (BOF) slag for supplementary cementitious materials.* Resources, Conservation and Recycling, 2018. **129**: p. 209-218.
31. Farrell, R.F., S.A. Matthes, and A.J. Mackie, *Simple, low-cost method for the dissolution of metal and mineral samples in plastic pressure vessels*. 1980, Bureau of Mines, Washington, DC (USA).
32. Justs, J., et al., *Influence of superabsorbent polymers on hydration of cement pastes with low water-to-binder ratio.* Journal of Thermal Analysis and Calorimetry, 2014. **115**(1): p. 425-432.
33. Hu, J., Z. Ge, and K. Wang, *Influence of cement fineness and water-to-cement ratio on mortar early-age heat of hydration and set times.* Construction and Building Materials, 2014. **50**: p. 657-663.
34. ASTM, *C109/C109M-16a Standard Test Method for Compressive Strength of Hydraulic Cement Mortars (Using 2-in. or [50-mm] Cube Specimens)*. 2016, ASTM: West Conshohocken, PA, 19428, United States.
35. Eberl, D.D., *User's Guide to Rockjock -- A Program for Determining Quantitative Mineralogy from Powder X-Ray Diffraction Data*, U.S.G.S., Editor. 2003, USGS: **Boulder, Colorado, USA**. p. 55.
36. Mertens, G., E. Zeelmaekers, and L. Machiel, *Use of quantitative X-ray diffraction for academic and industrial applications.* Acta Crystallographica, Section A. A, 2006. **62**: p. s209.
37. Eberl, D., *Quantitative mineralogy of the Yukon River system: Changes with reach and season, and determining sediment provenance.* American Mineralogist, 2004. **89**(11-12): p. 1784-1794.
38. Yoon, S., et al., *Phase changes of monosulfoaluminate in NaCl aqueous solution.* Materials, 2016. **9**(5): p. 401.
39. ASTM, *C1679-17: Standard Practice for Measuring Hydration Kinetics of Hydraulic Cementitious Mixtures Using Isothermal Calorimetry*. 2017, ASTM: West Conshohocken, PA, 19428, United States. p. 15.

40. Tashiro, C. and J. Oba, *The effects of Cr2O3, Cu (OH) 2, ZnO and PbO on the compressive strength and the hydrates of the hardened C3A paste.* Cement and Concrete Research, 1979. **9**(2): p. 253-258.
41. Chen, Q., et al., *Immobilisation of heavy metal in cement-based solidification/stabilization: a review.* Waste management, 2009. **29**(1): p. 390-403.
42. Mangabhai, R., *Calcium Aluminate Cements: Proceedings of a Symposium dedicated to HG Midgley, London, July 1990*. 2014: CRC Press.
43. Weeks, C., R.J. Hand, and J.H. Sharp, *Retardation of cement hydration caused by heavy metals present in ISF slag used as aggregate.* Cement and concrete composites, 2008. **30**(10): p. 970-978.
44. Wang, G.C., *The utilization of slag in civil infrastructure construction*. 2016: Woodhead Publishing.
45. Monkman, S., Y. Shao, and C. Shi, *Carbonated ladle slag fines for carbon uptake and sand substitute.* Journal of materials in civil engineering, 2009. **21**(11): p. 657-665.
46. Gineys, N., G. Aouad, and D. Damidot, *Managing trace elements in Portland cement–Part I: Interactions between cement paste and heavy metals added during mixing as soluble salts.* Cement and Concrete Composites, 2010. **32**(8): p. 563-570.
47. Stutzman, P.E. and J.R. Clifton. *Specimen preparation for scanning electron microscopy*. in *Proceedings of the international conference on cement microscopy*. 1999. International Cement Microscopy Association.
48. Scrivener, K., R. Snellings, and B. Lothenbach, *A Practical Guide to Microstructural Analysis of Cementitious Materials*. 2016: Crc Press.
49. Steinour, H.H., *Concrete Mix Water--How Impure Can It Be?* 1960.
50. Kakali, G., S. Tsivilis, and A. Tsialtas, *Hydration of ordinary portland cements made from raw mix containing transition element oxides.* Cement and concrete research, 1998. **28**(3): p. 335-340.
51. Chen, L., et al. *Crystal Structure and Hydration Characteristics of Tricalcium Silicate Doped with Magnesium Oxide*. in *Advanced Materials Research*. 2014. Trans Tech Publ.
52. Fajun, W., M.W. Grutzeck, and D.M. Roy, *The retarding effects of fly ash upon the hydration of cement pastes: The first 24 hours.* Cement and Concrete Research, 1985. **15**(1): p. 174-184.

53. Jiang, Y., et al., *Characteristics of steel slags and their use in cement and concrete—A review.* Resources, Conservation and Recycling, 2018. **136**: p. 187-197.
54. Yuji, W., *The effect of bond characteristics between steel slag fine aggregate and cement paste on mechanical properties of concrete and mortar.* MRS Online Proceedings Library Archive, 1987. **113**.
55. Wiesława, N.-W., T. Barbara, and D. Sylwia, *The properties of cement pastes and mortars processed with some heavy metal nitrates containing solutions.* Procedia Engineering, 2015. **108**: p. 72-79.
56. Gineys, N., G. Aouad, and D. Damidot, *Managing trace elements in Portland cement – Part I: Interactions between cement paste and heavy metals added during mixing as soluble salts.* Cement and Concrete Composites, 2010. **32**(8): p. 563-570.
57. Wang, Q., P. Yan, and J. Feng, *A discussion on improving hydration activity of steel slag by altering its mineral compositions.* Journal of hazardous materials, 2011. **186**(2-3): p. 1070-1075.
58. Shi, Y., et al., *Preliminary investigation on the pozzolanic activity of superfine steel slag.* Construction and Building Materials, 2015. **82**: p. 227-234.
59. Pacheco-Torgal, F., et al., *Handbook of alkali-activated cements, mortars and concretes*. 2014: Elsevier.
60. Najimi, M., N. Ghafoori, and M. Sharbaf, *Alkali-activated natural pozzolan/slag mortars: A parametric study.* Construction and Building Materials, 2018. **164**: p. 625-643.
61. Pang, B., Z. Zhou, and H. Xu, *Utilization of carbonated and granulated steel slag aggregate in concrete.* Construction and Building Materials, 2015. **84**: p. 454-467.
62. Muhmood, L., S. Vitta, and D. Venkateswaran, *Cementitious and pozzolanic behavior of electric arc furnace steel slags.* Cement and Concrete Research, 2009. **39**(2): p. 102-109.
63. Kim, D.-H., et al., *Removal mechanisms of copper using steel-making slag: adsorption and precipitation.* Desalination, 2008. **223**(1-3): p. 283-289.
64. Mahdavi, S., M. Jalali, and A. Afkhami, *Removal of heavy metals from aqueous solutions using Fe 3 O 4, ZnO, and CuO nanoparticles*, in *Nanotechnology for sustainable development*. 2012, Springer. p. 171-188.

65. Tamez, C., R. Hernandez, and J. Parsons, *Removal of Cu (II) and Pb (II) from aqueous solution using engineered iron oxide nanoparticles.* Microchemical Journal, 2016. **125**: p. 97-104.

66. Dimitrova, S. and D. Mehandgiev, *Lead removal from aqueous solutions by granulated blast-furnace slag.* Water Research, 1998. **32**(11): p. 3289-3292.